University College Cork, Ireland
Coláiste na hOllscoile Corcaigh

Size-Dependent Bandwidth of Semipolar $(11\bar{2}2)$ Light-Emitting-Diodes

M. Haemmer, B. Roycroft, M. Akhter, D. V. Dinh, Z. Quan, J. Zhao, P. J. Parbrook, and B. Corbett

Abstract—The limited modulation bandwidth of commercial light-emitting diodes (LEDs) is one of the critical bottlenecks for visible light communications. Possible approaches to increase the bandwidth include the use of micron sized LEDs, which can withstand higher current densities, as well as the use of LED structures that are grown on different crystal planes to the conventional polar c-plane. We compare c-plane InGaN/GaN LEDs with semipolar $(11\bar{2}2)$ LEDs containing a 4- and 8-nm single quantum well. The modulation bandwidth of semipolar LEDs with active areas varying from 200 × 200 to 30 × 30 μm^2 is shown to be governed by both current density and size. A small signal bandwidth of over 800 MHz for a relatively low applied current density of 385 A/cm^2 is reported for 30 × 30 μm^2 LEDs with 8-nm thick quantum well. An optical link using an easy non-return-to-zero ON–OFF keying modulation scheme with a data rate of 1.5 Gb/s is demonstrated.

Index Terms—Visible light communications, visible LED, semipolar GaN, modulation bandwidth.

I. INTRODUCTION

VISIBLE Light Communications (VLC) is an exciting emerging technology that can provide additional communication channels to those of radio frequency (RF) wireless communications. In contrast to RF based solutions, VLC offers the advantages of license-free operation, a much higher available frequency bandwidth and enhanced security due to the confinement of the signal to the room. Additionally, VLC generates no electromagnetic interference with RF devices [1]–[5]. A very attractive feature is the use of low-cost and increasingly ubiquitous light-emitting diodes (LEDs). Unlike lasers, LEDs have no threshold resulting in low power consumption, provide wavelength multiplexing opportunities and compatibility with current solid-state lighting systems [5]. Among several challenges hampering the development of VLC systems especially for high data rates is the limited modulation bandwidth of commercial c-plane InGaN LEDs which typically do not exceed 10-20 MHz. This bandwidth

can be further decreased when using phosphor converted white LEDs due to the slow phosphor response.

Improvements in the transmission bandwidth can be achieved by using complex modulation formats, parallel data transmission and equalisation [6]–[8] with increasing overhead on data processing. Alternatively, the bandwidth can be increased by using smaller devices and driving high current densities where bandwidths of up to 800 MHz for c-plane LEDs have been achieved by reducing the active area to 100 × 100 μm^2 or less [9]–[11]. Another approach is the use of semi- or non-polar LEDs that, due to the increased overlap of the electron and hole wave-functions, the radiative recombination rate is increased and bandwidths of 500 MHz for nonpolar [12] and 1 GHz for semipolar $(11\bar{2}2)$ InGaN/GaN LEDs have been obtained [13].

In this work, we study the size dependence of the bandwidth of 4-nm and 8-nm-thick single quantum well (SQW) LEDs realised on the $(11\bar{2}2)$ crystal plane. We show a considerable increase in bandwidth for these LEDs when compared to c-plane LEDs and that the $(11\bar{2}2)$ devices with the wider QW have the higher bandwidth. We use these $(11\bar{2}2)$ LEDs to show data transmission at data rates of 1.5 Gb/s while c-plane LEDs only reach 200 Mb/s under comparable conditions.

II. THEORY

The limitation of the modulation bandwidth for LEDs is associated with several factors which are encapsulated in the carrier lifetime, τ, and the associated cut-off or −3 dB frequency, f_{-3dB}, following the equation:

$$f_{-3dB} = \frac{\sqrt{3}}{2\pi\tau} = \frac{\sqrt{3}}{2\pi}\left(\frac{1}{\tau_R} + \frac{1}{\tau_{NR}} + \frac{1}{\tau_{RC}}\right). \qquad (1)$$

Consequently, the bandwidth is either limited by the carrier radiative lifetime, τ_R, the non-radiative lifetime, τ_{NR}, or the RC time constant ($\tau_{RC} = R \cdot C$) consisting of the differential resistance and parasitic geometric capacitance of the LED. For LEDs with sizes of 100 × 100 μm^2 and less the carrier radiative lifetime is reported to be the dominant factor limiting the modulation bandwidth [6], [14]. In this case, the carrier radiative lifetime depends on the current density injected into the LED since $\tau_R = 1/B \cdot N$, where N is the carrier density and B is the radiative recombination coefficient. An increase in current density, J, increases N. Assuming a bimolecular recombination mechanism, f_{-3dB}, follows the equation

$$f_{-3dB} = \frac{1}{2\pi}\sqrt{\frac{3BJ}{qt}} \sim J^{0.5}, \qquad (2)$$

where q is the elementary charge and t is the thickness of the active layer. Micron sized LEDs can withstand higher current densities due to less self-heating [14] resulting in higher carrier densities and reduced carrier lifetimes. Further, the reduction in active area leads to a decrease in geometric capacitance preventing the RC time constant becoming the dominating factor. The additional increase in modulation bandwidth for LEDs grown on semi- or non-polar substrates corresponds to an increase in the effective B.

III. DEVICE STRUCTURE AND FABRICATION

Semipolar $(11\bar{2}2)$ InGaN/GaN LEDs emitting at 440-450 nm were grown by metal organic vapour phase epitaxy on high quality $(11\bar{2}2)$ GaN templates with low basal plane stacking fault density. The templates were created on structured r-plane sapphire substrates [15]. Here, we study two LED structures each of which contains either a 4-nm or an 8-nm thick SQW. A reference c-plane wafer with 5 QWs was processed simultaneously. Substrate-emitting LEDs were fabricated by evaporating 50-nm thick Pd as the p-type contacts which define the emitting area and the device dimensions quoted in this letter. The device dimension ranged from 200×200 μm^2 to 20×20 μm^2. Mesas, sized by 3 μm with respect to the p-contacts were etched into the n-side of the junction where an n-type contact of Ti/Al/Ni/Au (20/50/10/200 nm) was deposited. An oxide passivation layer was deposited followed by opening to the p- and n-contacts and the evaporation of a bond metal with the pads aranged for high-speed ground-signal probing. The sapphire substrate was polished and a 70-nm thick layer of SiO$_2$ was sputter deposited to act as a partial antireflection coating. The electrical properties of the p-contacts show that the p-contacts to both semipolar samples are non-ohmic. The contacts to the c-plane sample were ohmic with a measured contact resistivity of 0.022 Ωcm^2 and p-layer sheet resistance of 328 kΩ. The peak emission wavelengths under electroluminescence are 439 nm, 449 nm and 469 nm for the 4-nm SQW, the 8-nm SQW and the c-plane devices, respectively.

IV. RESULTS AND DISCUSSION

The light-current-voltage (LIV) characteristics of the devices from the three wafers were measured using a photodetector with a numerical aperture (NA) of 0.5. The characteristics differ distinctly between the semipolar and the polar samples. Figure 1 shows the measured LIV characteristics for 100×100 μm^2 LEDs from each material. The differential resistances derived from this plot are around 50 Ω for the c-plane sample and around 240 Ω and 187 Ω for 4-nm SQW and 8-nm SQW LEDs, respectively. All structures show an increase in the turn-on voltage (V_{ON}) with decreasing active area that is more pronounced for the semipolar samples. For the 4-nm SQW LEDs V_{ON} varies from 4.5 V for the 200×200 μm^2 device to 8.5 V for the 20×20 μm^2 device while the corresponding variation for the 8 nm SQW LEDs is 3.5 V to 7.0 V and 2.5 V to 3.5 V for the c-plane devices. This increase for the semipolar devices occurs due to the poorer p-contact quality and will result in a higher heat load in comparison to the c-plane devices. This is not fundamental
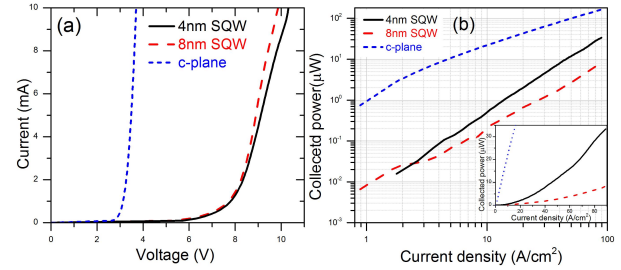

Fig. 1. Characteristics of 100×100 μm^2 LEDs from all three materials: (a) the current voltage characteristics, (b) the collected optical power against the applied current density on a log-log scale. The inset in (b) shows the same data on a linear scale. A detector with a numerical aperture of 0.5 was used.
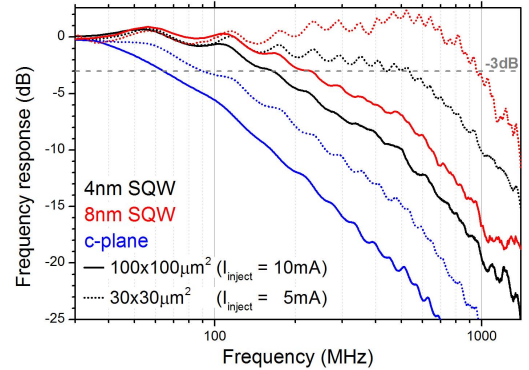

Fig. 2. Frequency response from all three materials at current densities of 89 A/cm^2 and 386 A/cm^2 relating to device sizes of 100×100 μm^2 and 30×30 μm^2.

as high efficiency, low resistance semipolar LEDs have been demonstrated [16].

The optical output power, P$_{\text{opt}}$, shown in Fig. 1 (b), is lower for the 4-nm SQW and 8-nm SQW devices in comparison to the more mature c-plane devices. This is partly due to the presence of Shockley-Read-Hall non-radiative recombination at low current densities (Inset of Fig. 1 (b)). These defect-related processes are observed to saturate and P$_{\text{opt}}$ increases with a higher differential internal quantum efficiency than for the c-plane sample under higher injection currents. While the absolute P$_{\text{opt}}$ is reduced for the smaller devices due to the reduced emission area, the power per unit area scales with current density for all device sizes.

The small-signal bandwidth of all LEDs was measured using a vector network analyser (VNA) and a high bandwidth silicon p-i-n photodiode with integrated transimpedance amplifier. A high-performance ground-signal microwave probe (DC to 3.5 GHz) was used to contact the LEDs without a heat sink. On top of a varying DC bias, an AC signal with a peak-to-peak voltage (V$_{\text{PP}}$) of 10 mV was applied using a bias tee. The light output of the LEDs was collected by two 2-cm-diameter lenses (NA = 0.5) and focussed on the photoreceiver. The frequency response curve was recorded for varying injection current and for frequencies from 10 kHz to 1.4 GHz limited by the photoreceiver. In Fig. 2 exemplary frequency response plots measured on two different device sizes (100×100 μm^2 and 30×30 μm^2) for all three LED materials are shown. The frequency response is enhanced at higher current density.

Notably, the semipolar samples show much higher response at high frequency when compared to the c-plane LED
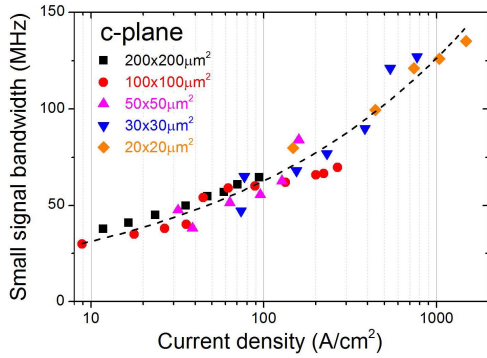
Fig. 3. Dependence of the small signal bandwidth on current density for c-plane devices. The data is fit (dashed curve) with a power law $f_{-3dB} \sim J^n$ with n = 0.303.
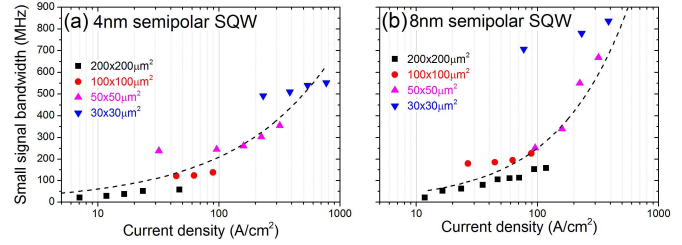

Fig. 4. Small signal bandwidth as a function of current density, J, and size for (a) 4-nm SQW and (b) 8-nm SQW semipolar samples: The data is fitted with a power law $f_{-3dB} \sim J^n_{inject}$ with n = 0.539 and n = 0.741 for the 4-nm SQW and 8-nm SQW, respectively.

and particularly the 8-nm SQW LEDs shows the highest frequency response. Small frequency oscillations ($\sim$60 MHz) and a response above 0dB are observed which are due to RF signal reflections in the transmission line especially for the semipolar devices. An increased frequency response for the 30×30 μm^2 8-nm SQW device at higher current densities is observed. Such enhancements are usually related to the relaxation resonance frequency in laser diodes but are not expected in LEDs. Using circuit simulations, it is possible to reproduce this increase in the high frequency response with passive circuit behaviour. A p-n junction contains resistance and capacitance that act as a low pass filter (LPF). If a LPF is preceded by a series capacitance with parallel resistance, effectively a shunted high-pass filter, then a high frequency peak can be obtained. While this extra capacitance may be due to a slightly non-ohmic metal-semiconductor contact, further investigation of this phenomenon is needed.

Figure 3 presents the dependence $f_{-3 dB}$ on J, for the c-plane LEDs. A power law of $f_{-3 dB} \sim J^n$ with n = 0.303 $\pm$ 0.014 is measured which is less than n = 0.5 expected from equation (2). The continual increase in $f_{-3 dB}$ with increasing J, implies it is not dominated by the RC time constant. There is no explicit dependence of $f_{-3 dB}$ on the size of the devices as, at the same J, different sized devices show equal $f_{-3 dB}$. Similarly, the $f_{-3 dB}$ values rise with J for each device size in both the semipolar materials as shown in Fig. 4. Hence, we can again conclude that the RC time constant is not the limiting factor. The semipolar LEDs show much higher $f_{-3 dB}$ values compared to their polar counterparts. The highest bandwidths of >800 MHz are achieved for the 8-nm SQW devices with a 30×30 μm^2 emitting area. This increase can be explained by the faster recombination due to the enhanced overlap of the electron and hole wave-functions in semipolar LEDs. It should be noted that with faster recombination it is expected that the carrier density in the active region is also less than for the c-plane for a given current density injected into the device. Furthermore, we can expect that the carrier density will be lower in the wider QW material, and this suggests that carrier density is not the only defining parameter for $f_{-3 dB}$. It should be noted that the 20×20 μm^2 devices of both semipolar LEDs yielded poor small signal response due to their low absolute optical output and the non-ohmic p-contacts.

In contrast to the continuous behaviour of $f_{-3 dB}$ for the c-plane LED, both semipolar samples show a step-like size dependent increase in modulation bandwidth for smaller devices (See Fig. 4). For example, $200 \times 200\mu$m^2, 100×100 μm^2 and 50×50 μm^2 sized LEDs processed from the 4-nm SQW sample at a current density around 40 A/cm^2 show modulation bandwidths of 57 MHz, 122 MHz and 238 MHz, respectively. A similar observation is made for 200×200 μm^2, 100×100 μm^2, 50×50 μm^2 and 30×30 μm^2 sized LEDs from the 8-nm SQW sample at a current density of $\sim$90 A/cm^2 where the cut-off frequencies are 153 MHz, 227 MHz, 252 MHz and 707 MHz, respectively. Consequently, the $f_{-3 dB}$ of these semipolar devices is governed by both the applied current density and the physical size of the active area. The enhancement is not related to a change in light output as the same injected current densities show similar optical power densities regardless of the device size. The smaller devices have higher perimeter to area ratio and electric fields with in-plane components may be expected at the etched sidewalls of semipolar devices. However, we found no evidence for this, as LEDs with equal emitting areas but different geometrical shapes and different sidewall lengths showed no distinct deviations in the cut-off frequency or in their LIV characteristics.

The high modulation bandwidths in the semipolar devices are obtained in spite of the high driving voltage across the devices resulting in electrical power densities of up to 6 kW/cm^2 with an expected strong rise in junction temperature. It should be noted that the substantial increase of the $f_{-3 dB}$ for the semipolar LEDs compared to their polar counterparts is not related to defects, since the very high $f_{-3 dB}$ are obtained in a region of high differential efficiency.

The inbuilt electric fields are a major factor in determining the bandwidth. The direction of the small inbuilt polarization electric field across the QWs in $(11\overline{2}2)$ devices is opposite to that in c-plane devices [18]. Another characteristic of the QWs grown on the $(11\overline{2}2)$ plane is a very strong exciton localisation effect which is observed even above room temperature [17].

Comparing the two semipolar samples in Fig. 4, the dependence of the f_{-3dB} on current density can be approximated with a power law $f_{-3dB} \sim J^n$ with n = 0.539 $\pm$ 0.066 and n = 0.741 $\pm$ 0.108 for the 4-nm SQW and 8-nm SQW, respectively. It is clear that the 8-nm SQW shows higher small signal bandwidth for a given current density. Based on equation (2), the opposite would be expected.
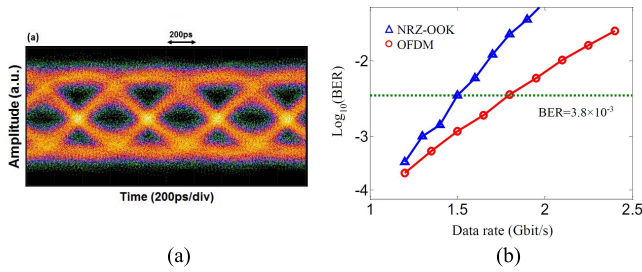
Fig. 5. (a): Eye diagram at a data rate of 1.5 Gb/s for a 50×50 μm^2 (11$\bar{2}$2) 8-nm SQW LED measured at I = 10 mA (J = 319 A/cm^2) using a 2^7-1 non-return-to-zero on-off-keying (NRZ-OOK) pseudo-random bit sequence. (b) BER versus the data rate of NRZ-OOK and OFDM signals.

Finally, a large signal bandwidth measurement was carried out in order to show that the LEDs can be used for actual data transmission. Therefore, the VNA was exchanged for a pattern signal generator on the transmitter side and a digital oscilloscope on the receiving end. A non-return-to-zero on-off keying (NRZ-OOK) pseudo-random bit sequence (PRBS) was applied and the large signal properties/back-to-back data transmission rates (i.e. eye diagrams) were recorded. Figure 5 (left) shows the eye diagram at a data rate of 1.5 Gb/s of a 50×50 μm^2 8-nm SQW device measured at an injection current of 10 mA, i.e. J = 319 A/cm^2. The measured small signal bandwidth is 668 MHz. We then measured the bit error rates (BER) for an advanced orthogonal frequency division multiplexing (OFDM) signal. An arbitrary waveform generator with varying sampling rate was used to generate the NRZ-OOK or the OFDM signal. The digital oscilloscope was replaced by a real-time oscilloscope with a sampling rate of 6.25 GSamples/s. The OOK signal consisted of a repetitive PRBS with a pattern length of 2^{15}-1 and data decision was made using optimal threshold detection at the centre of the eye diagram. In OFDM, 128 subcarriers were employed: the DC and the last subcarriers were zero-padded; 63 subcarriers were modulated with data while the remaining 63 subcarriers were used for Hermitian conjugation to generate a real-valued signal for intensity modulation. Signal levels of subcarriers are adaptively loaded according to the channel frequency response, with higher signal levels at low-frequency subcarriers and lower signal levels at high-frequency ones [18].

The driving signal voltages of the LED were optimized to balance the signal-to-noise ratio and the nonlinearity of LEDs, and were found to be 1.45 V and 1.6 V for NRZ-OOK and OFDM, respectively. Figure 5(right) shows the measured BER versus the data rate at back-to-back. It is seen that our LEDs could support 1.5 Gbit/s NRZ-OOK and 1.8 Gbit/s OFDM signal at a BER of 3.8×10^{-3}. This significantly outperformed the c-plane LEDs, where similar quality was obtained at data rates of only 200 Mb/s. Thus, by using these semipolar LEDs, a high data rate with a relatively low current density and simple signalling was achieved. Future work will focus on this option to reach higher data rates, where c-plane micro-LEDs as well as commercial white LEDs have achieved enhanced high data rates using this technique.

V. CONCLUSIONS

We have shown that the modulation bandwidth for semipolar (11$\bar{2}$2) InGaN/GaN LEDs is strongly increased over c-plane devices at a given current density. The bandwidth increases with current density with a power law dependence which increases from 0.3 (for c-plane) to 0.54 (for the 4-nm-thick SQW) to 0.74 for the 8-nm-thick SQW. The semipolar LEDs also show higher bandwidth for smaller devices at a given current density. The LEDs reach cut-off frequencies above 800 MHz and have been used to demonstrate 1.5-Gb/s and 1.8-Gb/s data links using NRZ-OOK and OFDM modulation schemes, respectively. These devices have the potential to overcome the problem of limited bandwidth in visible light communication with conventional c-plane devices.

REFERENCES

[1] H. Elgala, R. Mesleh, and H. Haas, "Indoor optical wireless communication: Potential and state-of-the-art," *IEEE Commun. Mag.*, vol. 49, no. 9, pp. 56–62, Sep. 2011.

[2] C.-X. Wang *et al.*, "Cellular architecture and key technologies for 5G wireless communication networks," *IEEE Commun. Mag.*, vol. 52, no. 2, pp. 122–130, Feb. 2014.

[3] G. C. García *et al.*, "State of the art, trends and future of Bluetooth low energy, near field communication and visible light communication in the development of smart cities," *Sensors*, vol. 16, no. 11, p. 1968 2016.

[4] J. Grubor, S. Randel, K.-D. Langer, and J. W. Walewski, "Bandwidth-efficient indoor optical wireless communications with white light-emitting diodes," in *Proc. 6th Int. Symp. Commun. Syst., Netw. Digit. Signal Process.*, vol. 1. Graz, Austria, Jun. 2008, pp. 165–169.

[5] S. Rajbhandari *et al.*, "A review of gallium nitride LEDs for multi-gigabit-per-second visible light data communications," *Semicond. Sci. Technol.*, vol. 32, no. 2, p. 023001, 2017.

[6] D. Tsonev *et al.*, "A 3-Gb/s single-LED OFDM-based wireless VLC link using a gallium nitride μLED," *IEEE Photon. Technol. Lett.*, vol. 26, no. 7, pp. 637–640, Apr. 1, 2014.

[7] A. H. Azhar, T. Tran, and D. O'Brien, "A gigabit/s indoor wireless transmission using MIMO-OFDM visible-light communications," *IEEE Photon. Technol. Lett.*, vol. 25, no. 2, pp. 171–174, Jan. 15, 2013.

[8] Y. Hong, L.-K. Chen, and J. Zhao, "Experimental demonstration of performance-enhanced MIMO-OFDM visible light communications," in *Proc. Opt. Fiber Commun. Conf. Exhibit. (OFC)*, 2017, pp. 1–3.

[9] R. X. G. Ferreira *et al.*, "High bandwidth GaN-based micro-LEDs for multi-Gb/s visible light communications," *IEEE Photon. Technol. Lett.*, vol. 28, no. 19, pp. 2023–2026, Oct. 1, 2016.

[10] C.-L. Liao, C.-L. Ho, Y.-F. Chang, C.-H. Wu, and M.-C. Wu, "High-speed light-emitting diodes emitting at 500 nm with 463-MHz modulation bandwidth," *IEEE Electron Device Lett.*, vol. 35, no. 5, pp. 563–565, May 2014.

[11] J.-W. Shi, K.-L. Chi, J.-M. Wun, J. E. Bowers, Y.-H. Shih, and J.-K. Sheu, "III-nitride-based cyan light-emitting diodes with GHz bandwidth for high-speed visible light communication," *IEEE Electron Device Lett.*, vol. 37, no. 7, pp. 894–897, Jul. 2016.

[12] A. Rashidi *et al.*, "High-speed nonpolar InGaN/GaN LEDs for visible-light communication," *IEEE Photon. Technol. Lett.*, vol. 29, no. 4, pp. 381–384, Feb. 15, 2017.

[13] D. V. Dinh, Z. Quan, B. Roycroft, P. J. Parbrook, and B. Corbett, "GHz bandwidth semipolar (11$\bar{2}$2) InGaN/GaN light-emitting diodes," *Opt. Lett.*, vol. 41, no. 24, pp. 5752–5755, 2016.

[14] Z. Gong *et al.*, "Size-dependent light output, spectral shift, and self-heating of 400 nm InGaN light-emitting diodes," *J. Appl. Phys.*, vol. 107, no. 1, p. 013103, 2010.

[15] F. Brunner *et al.*, "Semi-polar (11$\bar{2}$2)-GaN templates grown on 100 mm trench-patterned r-plane sapphire," *Phys. Status Solidi B*, vol. 252, no. 5, pp. 1189–1194, 2015.

[16] H. Li *et al.*, "Efficient semipolar (11$\bar{2}$2) 550 nm yellow/green InGaN light-emitting diodes on low defect density (11$\bar{2}$2) GaN/sapphire templates," *ACS Appl. Mater. Interfaces*, vol. 9, no. 41, pp. 36417–36422, 2017.

[17] D. V. Dinh, S. Presa, P. P. Maaskant, B. Corbett, and P. J. Parbrook, "Exciton localization in polar and semipolar (11$\bar{2}$2) In$_{0.2}$Ga$_{0.8}$N/GaN multiple quantum wells," *Semicond. Sci. Technol.*, vol. 31, no. 8, p. 085006, 2016.

[18] J. Zhao and L.-K. Chen, "Adaptively loaded IM/DD optical OFDM based on set-partitioned QAM formats," *Opt. Exp.*, vol. 25, no. 8, pp. 9368–9377, 2017.